Journal of the Optical Society of America B
OPTICAL PHYSICS

Scattering transmission field of a photonic crystal surface wave to determine the thickness distribution of thin films

F. Villa-Villa,[1,3] R. Cortés,[2] C. E. Garcia-Ortiz,[2,4] B. Reyes-Ramirez,[1] and V. Coello[2]

[1]Centro de Investigaciones en Óptica, Loma del Bosque 115, Lomas del Campestre, León Gto. 37150, Mexico
[2]CICESE, Unidad Monterrey, Alianza Centro 504, PIIT Apodaca, N.L. 66629, Mexico
[3]e-mail: fvilla@cio.mx
[4]e-mail: cegarcia@cicese.mx

Received 26 April 2019; revised 19 July 2019; accepted 25 July 2019; posted 26 July 2019 (Doc. ID 366044); published 21 August 2019

In present work, we use an electromagnetic surface mode excited at the interface of a finite one-dimensional photonic crystal utilizing a modified attenuated total reflection setup by capturing the images formed by the scattered surface waves under transmission to determine the thickness distribution of a non-uniform thin film (<100 nm) over an extended millimeter-sized area. The sensitivity of the proposed technique is analyzed by considering a step coating that presents two different regions of different thickness, which shifts the resonant conditions of the surface mode. © 2019 Optical Society of America

https://doi.org/10.1364/JOSAB.36.002526

1. INTRODUCTION

Some years after the invention of photonic crystals (PC), surface electromagnetic waves (SWs) that can exist at the interface between a semi-infinite one-dimensional photonic crystal (1DPC) and a bulk material or vacuum [1–3] were proposed to be applied in a sensing device based on attenuated total reflectance (ATR) in a similar way to surface plasmon polaritons (SPPs) on metals [4,5]. As with SPPs, the key idea behind these photonic sensors is to measure the optical properties of thin films and liquid substances [6] or to determine the presence of very thin layers of organic materials [7]. After the introduction of SWs on a sensing device, an analytical theory based on equivalent systems that compliments the numerical methods borrowed from solid-state physics like the plane waves method [3] was proposed to study the properties of SWs [8,9], and some experimental work to verify their existence was developed [10–13]. During the last 15 years, extensive work has been done on experimental analysis of SWs applied in the basic sensing device. Some of the more recent work can be found in Refs. [14,15]. In recent years, a comparative analysis between SWs and SPPs using the sensitivity as a point of view has been proposed by Sinibadi *et al.* [15]. An interesting application of SWs as the basis for an atomic force microscope has been considered by Shilkin *et al.* [16]. Finally, another interesting application that seems a bit related to the method we are proposing here is the use of fluorescent substances deposited on top of a truncated 1DPC with a grating of rectangular groves [17]. The idea is to excite the fluorescent substance, which emits in the range of frequencies of two different SWs corresponding to the top and the bottom of each grove. Although this technique discriminates between two different thicknesses of a structured material constituting the grating, it has not been tested to analyze the morphology of systems over an extended area.

It is worth mentioning that in contrast to SPPs, SWs present some important advantages in sensing devices based on the ATR configuration, since the PCs necessary to support the surface modes are built from highly stable dielectric materials that are not very susceptible to degradation even after a number of different tests, as eventually happens with metallic thin films. The 1DPC-bulk system can be constructed to present SWs at any frequency of the electromagnetic spectrum in both polarizations, and their sensitivity can be manipulated depending on many factors such as the truncation of the layer in contact with the bulk material, the extinction coefficient of composing dielectric layers, and the number of periods of the finite 1DPC. All these factors will affect the penetration depth of the electromagnetic waves within the PC and the decaying length along the surface; therefore, by managing them we can modify the sensitivity of this sensor. Quite recently also it has been experimentally observed that by analyzing the scattered transmission field of an extended area along the sample, it is possible to get essential information about a SPP and its perturbation in virtue of the presence of a variable thickness dielectric overlayer [18,19].

In this work we use a similar method but considering PC-bulk SWs instead, given some advantages those present over their plasmonic counterparts. In this context, a subtle property

that deserves to be emphasized in comparing SW with SPPs is the maximum overlayer thickness that can be measured. While with SPPs we are able to measure a layer thickness up to 100 nm, with SW the thickness of the sensed layer can be much larger, depending on the design of the PC and the region of the spectrum where the mode is located. Therefore, the contribution of this paper resides in presenting a technique for the measurement of the thickness distribution of a dielectric thin film along an extended area by using 1DPC-bulk SWs and the scattered light under transmission.

2. THEORY

As our results are based on the excitation of SWs at the 1DPC–air interface, let us state the basic theory to determine the band structures and the mathematical conditions that must be satisfied in order for SWs to exist. In the formalism of the characteristic matrix method of propagation of light through multiple layer systems [8], each thin film can be associated with a 2×2 matrix that is a function of the parameters of the jth film and the frequency of light ω as follows:

$$m(\eta_j, \delta_j) = \begin{bmatrix} \cos(\delta_j) & \frac{i}{\eta_j}\sin(\delta_j) \\ i\eta_j \sin(\delta_j) & \cos(\delta_j) \end{bmatrix}. \tag{1}$$

This characteristic matrix relates the electromagnetic fields from one medium to the next. In the last expression,

$$\delta_j = \frac{2\pi}{\Lambda}\overline{k}_{zj} t_j \tag{2}$$

represents the phase thickness,

$$\eta_j = \begin{cases} y\overline{k}_{zj}/\overline{\omega} & \text{TE polarization,} \\ y n_j^2 \overline{\omega}/\overline{k}_{zj} & \text{TM polarization} \end{cases} \tag{3}$$

stands for the optical admittance of the corresponding thin film, and

$$\overline{k}_{zj} = \sqrt{n_j^2 \overline{\omega}^2 - \overline{\beta}^2} \tag{4}$$

is the reduced perpendicular component (to the interfaces) of the wave vector. The constant y represents the optical admittance of a vacuum. Here $\overline{\omega} = \omega\Lambda/2\pi c$ and $\overline{\beta} = \beta\Lambda/2\pi$ represent the reduced frequency and the reduced parallel component of the wave vector, respectively. The constant Λ has the same dimensions as the thickness of layers and is a scaling constant, c is the speed of light in a vacuum, and n_j is the refractive index of the jth medium. The band structures in both polarizations can be determined by using the expression for the equivalent optical admittance function δ_e for an infinitely periodic system composed of a period of two layers p and q, respectively, as follows:

$$\cos(\delta_e) = \cos(\delta_p)\cos(\delta_q) - \rho^+ \sin(\delta_p)\sin(\delta_q), \tag{5}$$

where

$$\rho^+ = \frac{1}{2}\left(\frac{\eta_p}{\eta_q} + \frac{\eta_q}{\eta_p}\right). \tag{6}$$

The band gap boundaries exist at frequencies where δ_e changes from being a purely real to purely imaginary quantity (or vice versa) for a given value of the parallel component of the wave vector $\overline{\beta}$. On the other hand, SWs can exist at the interface of a truncated 1DPC in contact with a bulk material or vacuum. For example, if we consider a system of k periods plus one overlayer of a p material with phase thickness δ_p' (Fig. 1), the characteristic matrix of this multilayer will be

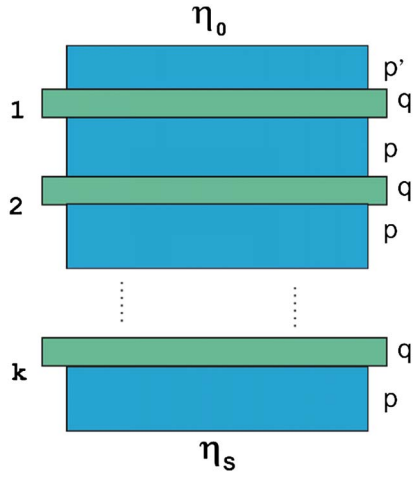

Fig. 1. Schematic description of the multilayer system.

$$\begin{bmatrix} M_{11} & M_{12} \\ M_{21} & M_{22} \end{bmatrix} = m(\eta_p, \delta_p')[m(\eta_q, \delta_q) m(\eta_p, \delta_p)]^k, \tag{7}$$

and the total optical admittance of the multilayer supported by a substrate medium of admittance η_s will be given by

$$Y = \frac{M_{21} + \eta_s M_{22}}{M_{11} + \eta_s M_{12}}. \tag{8}$$

Then, the condition for the existence of a SW at the 1DPC–air interface [8] corresponds to

$$Y = -\eta_0. \tag{9}$$

It can be demonstrated that a SW, which is a highly localized mode along a PC-bulk interface, must be located in regions of the dispersion diagram below the light line of air or a vacuum and within a band gap in order to exist [3,8]. In Fig. 2(a) we show the band structure under TE polarization of a 1DPC whose period is composed of two dielectric layers p and q with refractive indices and thicknesses $n_p = 2.37$, $t_p = 80.2$ nm, $n_q = 1.46$, and $t_q = 130.1$ nm, respectively. In this dispersion diagram we used the normalization constant $\Lambda = t_p + t_q$. Within the first band gap a SW is indicated by a dashed curve with spheres. In Fig. 1(b) the reflectance as a function of the wavelength in the region around the SW is graphed for a finite system with four periods $k = 4$ and an overlayer with $t_p' = 48$ nm, when the incidence medium is a BK7 optical glass under an incidence angle of 56°. In order to observe the SW, an absorption index of $k_p = 0.0117$ was assumed for the high index material.

One fact that deserves a particular explanation is the apparent existence of the SW outside of the first band gap. It is worth recalling that the edges of band gaps are determined for ideal infinitely periodic photonic crystals. However, when we deal with finite truncated systems composed of a few periods, the borders of band gaps become diffusely located and defined.

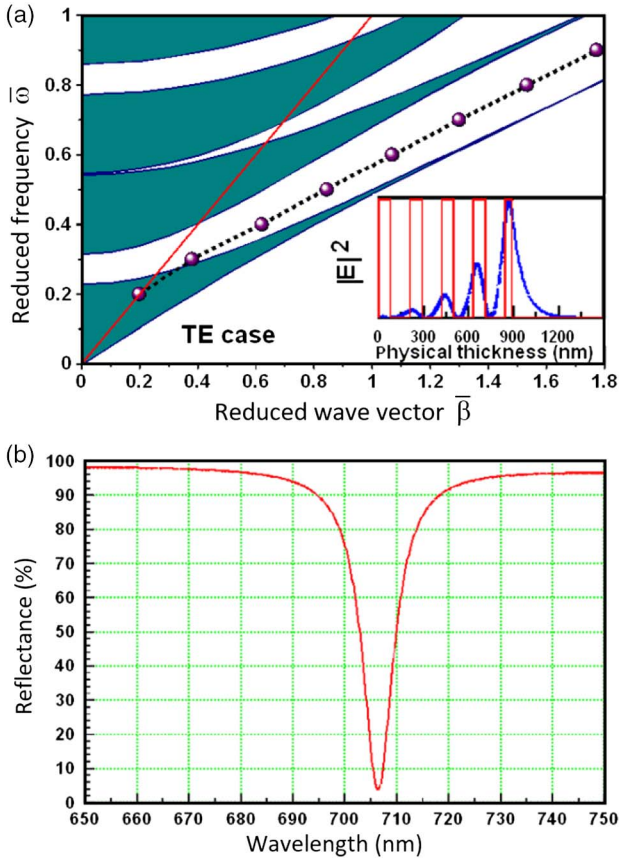

Fig. 2. (a) Band structure of 1DPC under TE polarization. Allowed bands are indicated by shaded regions and band gaps with white color. The light line for vacuum is shown with the red line. (b) Reflectance versus wavelength in the region around the SW for $\overline{\beta} = 0.375$ and $\overline{\omega} = 0.298$, which corresponds to $\theta = 56°$, and a wavelength $\lambda = 706.5$ nm, with an incident medium of $n_0 = 1.52$. The inset in (a) shows the intensity of the field at such point.

Despite this fact, the condition given above, $Y = -\eta_0$, guarantees the validity of our SW.

Additionally, we can verify that the SWs located apparently outside this band gap are real by calculating the field amplitude across the multilayer at the point of interest; for example, for the mode given in Fig. 2 located at $\overline{\beta} = 0.375$ and $\overline{\omega} = 0.298$, the field profile shown in the inset of Fig. 2(a) makes evident that the envelope at both sides of the air-(truncated) 1DPC is exponentially decaying. This is the main characteristic that defines a SW.

3. MATERIALS AND METHODS

The sample consists of a finite 1DPC prepared using a high-vacuum electron-beam evaporation system. The multilayer was deposited on a BK7 glass substrate, and it consisted of a periodic intercalated stack system of TiO_2 and SiO_2 thin films (eight layers in total) with thicknesses of 80.2 nm and 130.1 nm, respectively. An extra layer of TiO_2 was deposited on top of this finite 1DPC, but this time a step was created in the middle of the area to have different thicknesses at each half of the outermost layer of the sample. The step was fabricated by a two-run evaporation process that is described as follows: first, a layer of 48 nm of TiO_2 was deposited over the 1DPC, then one half of the sample was obstructed with a physical barrier to finally add an additional 17-nm-thick layer of TiO_2 on top [Fig. 3(a)]. The result consisted of a 1DPC divided in two regions, namely, zone 1 and 2, with the difference of the extra layers of fractional thicknesses $t_1 = 48$ and $t_2 = 65$ nm, respectively.

In order to observe a finite width deep at the mode frequency, some absorption was added to the TiO_2 layers by controlling a background oxygen pressure of about 10^{-5} mbar during the deposition of all the layers of this material. The optical constants of the deposited materials were characterized using UV-VIS spectrophotometer (Agilent spectrophotometer Cary 5000). The refractive indices determined by transmittance measurements were 1.46 and $2.38\text{-}0.0117i$ for the SiO_2 and TiO_2 films, respectively, along the range from 700 to 900 nm. For the purposes of this work, the 1DPC was designed to exhibit a photonic band gap within the wavelength range of 700–900 nm and taking into account the range of accessible wave vectors, given the physical constraints of the angle of incidence associated with the generation of evanescent waves and prism coupling.

The experimental configuration consists of a modified ATR setup (Fig. 4). The main modification permits a two-dimensional acquisition of the image produced by the scattered light at the surface of the sample. A charge-coupled device (CCD) camera and a system of lenses, which rotate along with

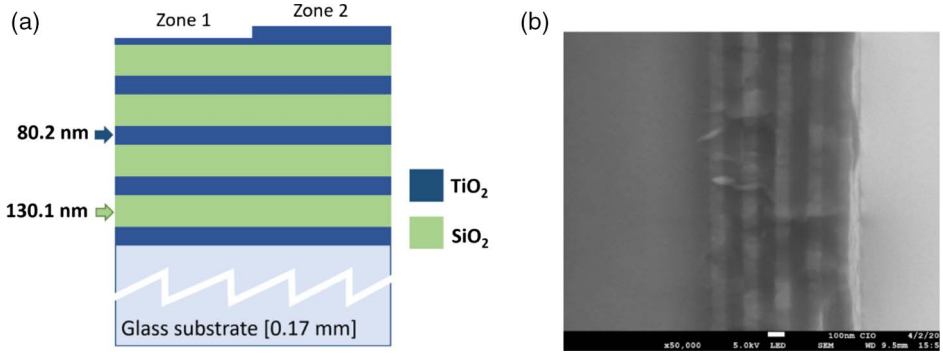

Fig. 3. (a) Schematic diagram of the fabricated sample. The top layer consists of two zones with a step difference of 17 nm and thicknesses $d_1 = 48$ and $d_2 = 65$ nm. (b) SEM image of the edge of our multilayer composed of 9 thin films: glass–4(p q)–p'–air.

the rotation stage, were used to store the images of the surface at each angle of incidence. The experiments were performed using a continuous-wave Ti:sapphire tunable laser (Spectra-Physics, model 3900S, 700–1000 nm) as the light source. The coupling prism consisted of a right-angle prism, where the sample was positioned on the hypotenuse face using index-matching oil. More details of the experimental setup can be consulted in [19], as it was used in a previous work to reconstruct the thickness distribution of a dielectric thin film using the scattering produced by SPPs.

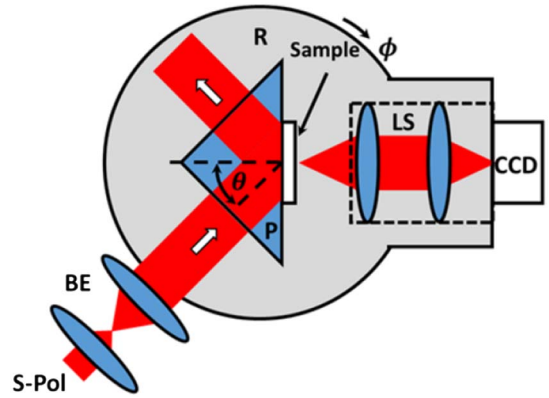

Fig. 4. Experimental setup for measuring the scattered transmitted field under the ATR configuration by using a CCD camera and an optical system (LS). A beam expander (BE) was used to illuminate the sample completely. The prism (P) moves along with the rotation stage (R) to image the same point at every angle.

4. RESULTS AND DISCUSSION

A. Numerical Calculations

The optical properties of the fabricated 1DPC were studied numerically. The reflectivity of the system, as a function of the wavelength and angle of incidence, was obtained using the characteristic matrix method for TE polarization. The calculations were performed using the fabrication parameters mentioned in the previous section as well as the estimated refractive index of the materials. The obtained reflectivity distributions show the presence of ATR for several combinations of $\overline{\omega}$ and $\overline{\beta}$, which are clear indications of the excitation of SW modes [Figs. 5(a)–5(d)]. More importantly, the calculations indicate that it is possible to excite a SW within the desired wavelength range and in the accessible angular interval for the available materials.

The reflectivity distributions were calculated for the two 1DPC systems with different top layers. The difference

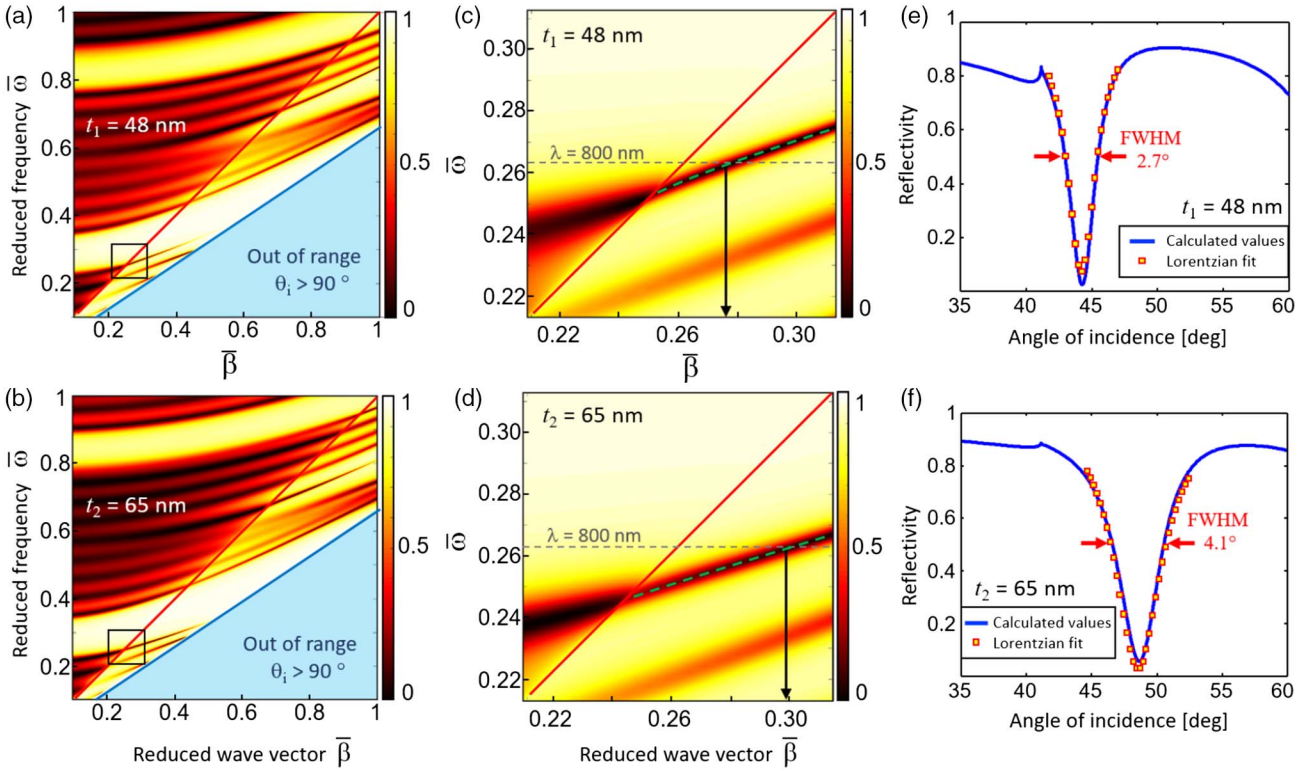

Fig. 5. (a)–(b) Calculated reflectivity of the finite 1D photonic crystals with truncated layers of (a) $t_1 = 48$ nm and (b) $t_2 = 65$ nm. The red line corresponds to the light line in a vacuum (critical angle), and the blue line delimits the inaccessible experimental range of $\theta_i > 90°$ (light blue region). Attenuated total reflection can be observed to the right of the light line of vacuum, showing the existence of evanescent surface modes. (c)–(d) Amplified images of (a) and (b). The dashed horizontal line corresponds to the wavelength used in our experiments $\lambda = 800$ nm ($\overline{\omega} = 0.262$). The black arrows indicate the value of $\overline{\beta}$ at the intersection of the minimum reflectivity with w. The green dashed line is a guide for the eye showing the calculated dispersion of the surface modes. (e)–(f) Cross sections of the reflectivity as a function of the angle of incidence at a wavelength of 800 nm for the photonic crystals of (a) and (b), respectively.

between the tops is better observed with a cross section along a specific frequency $\overline{\omega} = 0.2629$, which corresponds to $\lambda = 800$ nm [Figs. 5(e) and 5(f)]. The thickness of the outermost layer determines the position of the resonance (minimum reflection) with respect to the angle of incidence. The calculations show that for $t_1 = 48$ nm the coupling occurs at an angle $\theta_i = 44.1°$, and for $t_2 = 65$ nm the resonant coupling is observed at $\theta_i = 48.4°$. Bearing in mind that it is clear that the inverse process can be done, i.e., if the resonant coupling angle is known and so are all the physical and optical parameters of the 1DPC, it is possible to estimate the thickness of the top layer with high precision.

The propagation length can be estimated by measuring the full-width at half-maximum (FWHM) of the dip in the reflectance curves around the resonance angle for both the theoretical and numerical results by using an approximation for the reflectivity function based on the Lorentzian distribution [20]

$$R(\theta) = 1 - \frac{\text{const.}}{[k_x(\theta) - \beta']^2 + (\beta'')^2}, \tag{10}$$

where $k_x(\theta) = k_0 n_0 \sin(\theta)$ is the parallel component of the wave vector of the incident wave, β' is the real part of the SW wave vector, and β'' is its imaginary part. By fitting our reflectance curves given in Figs. 5(e) and 5(f) we have found that $\beta_1'' = 0.029 k_0$ and $\beta_2'' = 0.043 k_0$, respectively, where $k_0 = 2\pi/\lambda$ is the free-space wave vector. Therefore, the propagation length of the SWs in both cases is determined by the relation

$$L_{SW} = \frac{1}{2\beta''} \tag{11}$$

to be $L_{SW} = 2.2$ and $L_{SW} = 1.5$ μm, respectively. Although these propagation lengths could be perceived as relatively short compared to other typical Bloch SWs, this effect is explained by the fact that these SWs are located very close to the edge of the band gap. Therefore, the radiative losses represent the main mechanism of optical loss along propagation and the principal reason for the resonance broadening [21].

The finite-difference time-domain (FDTD) method was used to calculate the field and intensity distributions of the SW modes (Fig. 6). The simulation parameters consisted of an s-polarized illumination source with a wavelength of 800 nm, incident at two different angles of 44.1° and 48.4° for two top-layer thicknesses of 48 and 65 nm, respectively (at the resonance). These values were taken from the theoretical prediction and from the reflectivity results shown previously. From the field intensity distributions, it is possible to calculate the propagation length of the mode by taking an intensity profile along the direction of propagation x. The propagation length L_{SW} is defined as the distance where the SW mode

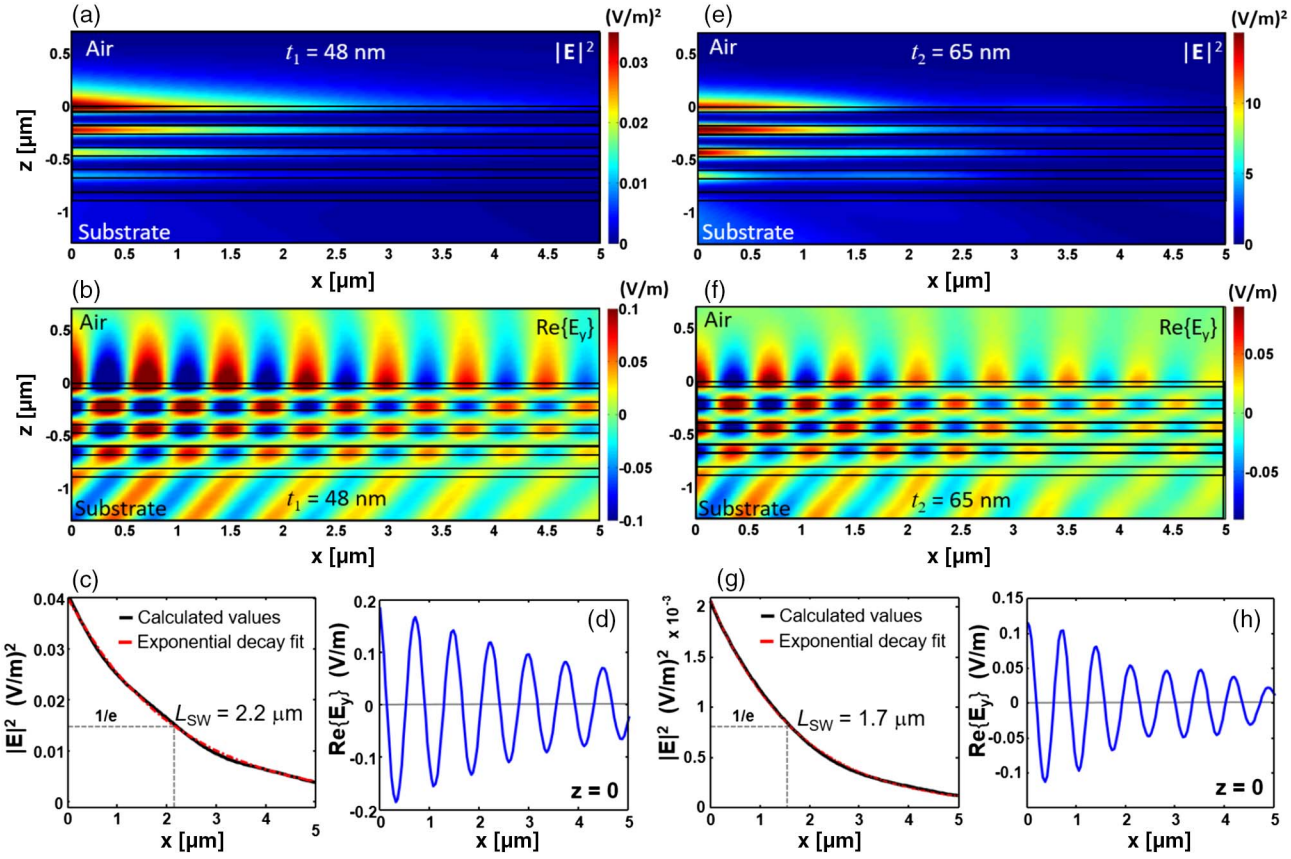

Fig. 6. (a)–(d) FDTD calculations for the top-layer thickness of 48 nm. (a) Electric-field intensity distribution $|\mathbf{E}(x,z)|^2$ and (b) real part of the transverse electric-field $\mathrm{Re}\{E_y(x,z)\}$ distribution. (c) Intensity and (d) field profiles along the propagation direction at the position $z = 0$. (e)–(h) FDTD calculations for the top-layer thickness of 65 nm. (e) Electric-field intensity distribution $|\mathbf{E}(x,z)|^2$ and (f) the real part of the transverse-electric field $\mathrm{Re}\{E_y(x,z)\}$ distribution. (g) Intensity and (h) field profiles along the propagation direction at the position $z = 0$.

intensity drops to $1/e$. The resulting lengths, $L_{SW}(48\ \text{nm}) = 2.2\ \mu\text{m}$ and $L_{SW}(65\ \text{nm}) = 1.7\ \mu\text{m}$, are in good agreement with the previously obtained values from the reflectivity calculations.

B. Experimental Results

First we characterized the average thickness of the two regions of the sample by comparing the experimental results with the numerical calculations. The resonant coupling angles were obtained using standard ATR measurements for the wavelength range of 740–800 nm with steps of 10 nm. The illumination laser-beam spot covered an area of ∼1 mm^2 and was set for s polarization [Fig. 7(a)]. The FWHMs of the measured resonance curves are ∼3° and 5° for t_1 and t_2, respectively. This results are in good agreement with the numerical calculations of Section 4.A. The relatively small broadening of the resonance is explained by the inherent surface roughness. The dispersion plot details the performance of the PC bandgap in the regions of interest and shows the average thickness of each zone. In this sample, the angle of minimum reflectivity decreases with increments of the wavelength and increases with the thickness of the outermost layer. The same results can be obtained if the scattered light is detected from the surface using our imaging system. In such case, the obtained measurements consist of peaks of maximum intensity produced by the scattered light associated with the field enhancement at the surface when coupling to the SWs [Fig. 7(b)]. The refractive index of the TiO_2 film was estimated from numerical fitting, yielding a value of $2.361 - 0.015i$.

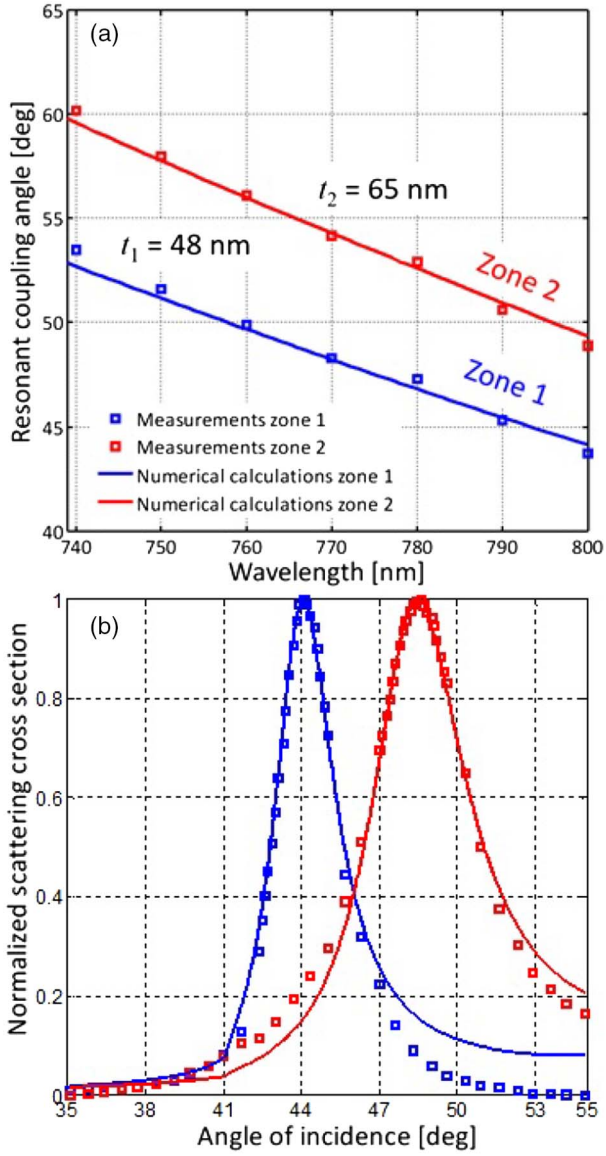

Fig. 7. (a) Experimental dispersion diagram and numerical fits showing the resonant coupling angle as a function of the free space excitation wavelength for the two zones of the sample. (b) Scattering measurements (squares) obtained with the CCD camera, and numerical fits (solid lines).

Now we focus on the main objective of this work, which is to get an estimation of the local point-by-point optical properties and reconstruct the thickness distribution of the dielectric layer deposited on top of the 1DPC. The images of the surface were taken at each angle in the angular range $\theta_i = 40$–$60°$. The sample was aligned to the imaging system in such way that the boundary between the two zones was at the center of the image. As the stage was rotated, it was possible to observe in the CCD camera how each half of the surface of the sample scattered the SWs around the resonance angles appeared as bright and dark regions (Fig. 8). These sets of images are further processed to get an estimate of the local thickness. Every pixel of the CCD camera is treated as an individual power detector, and a numerical fitting is processed for each using an automated MATLAB script. The algorithm finds the best fit, leaving the thickness as a fitting parameter. To improve the quality of the detected signal, an array of 3 × 3 physical pixels of the CCD camera were averaged, resulting in an optical lateral resolution of ∼12 μm. A complete description of the algorithm was reported in a previous work [18]. It is important to mention that the amplitude of the scattering cross section was also set as a fitting parameter to account for the different scattering local properties of the surface. The result is a three-dimensional thickness distribution of the top layer (Fig. 9). The reconstructed surface reveals the surface features of the fabricated sample. Each of the zones with different thicknesses are very clearly distinguishable, and so is the boundary between them. With this technique, it is even possible to observe the limitations of the fabrication technique with regards to the barrier used to divide each zone during evaporation, as it is possible to observe the irregular line that divides each zone. The latter is an indication of material filtrations though the edge of the barrier. The scattered light is not uniformly distributed in the image because the average local roughness is also not distributed homogenously over the surface. A combination of different grain sizes and geometries can significantly enhance or decrease the scattering cross sections. Nevertheless, the real part of the effective mode index of the SW, which determines the position of the maximum scattered light, remains unaltered with such small variations (1–5 nm) of the grain size on the surface, if compared to the overall film thickness. For these reasons, it is possible to observe brighter regions distributed in the image produced by the scattered light (Fig. 8), which are not present in the

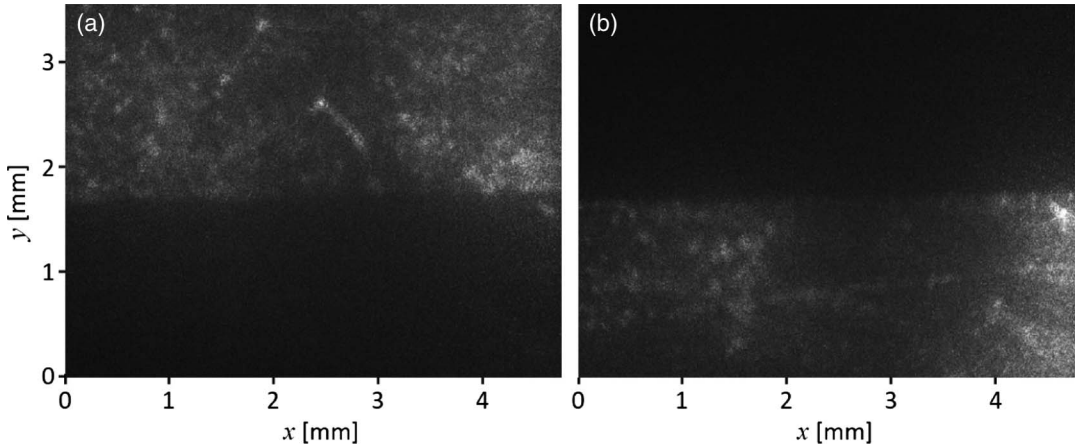

Fig. 8. Optical images of the 1DPC top-layer surface at the resonant coupling angles of incidence of (a) 44.1° and (b) 48.4°. The illuminated areas correspond to the scattering of SW produced by the surface roughness. The boundary between the two regions of the sample can be observed in the middle of both images with a different contrast. The imaged area has dimensions of 4.7 × 3.5 mm.

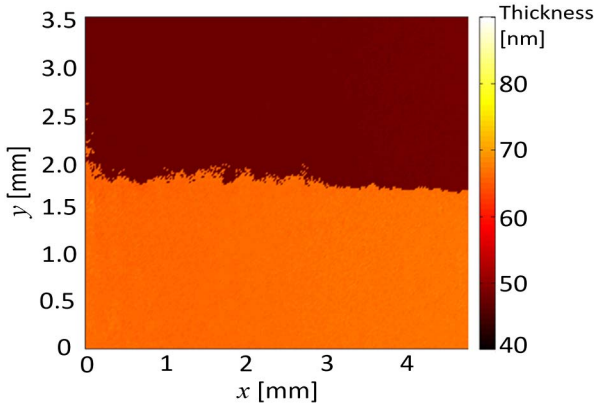

Fig. 9. Thickness distribution of the top layer of TiO_2.

thickness distribution (Fig. 9). The lateral resolution in this technique is fundamentally limited by the propagation length of the SWs, i.e., the resonance is not strictly local but weighted over at least one propagation length. Nevertheless, in this case, the propagation lengths of both modes (∼2 μm) are considerably smaller than our pixel size (∼12 μm), i.e., 6 times smaller than our optical resolution system. Therefore, the thickness distributions presented here can be considered local to this extent. It is worth mentioning that relatively large irregularities could in principle cause a shadowing effect that could cause distortions in the reconstructed thickness distribution, depending on the illumination direction. This last constitutes a limitation to the average roughness of the samples that could be mapped with this technique.

5. CONCLUSION

With this technique it is possible to reconstruct 3D thickness maps of dielectric thin films through the detection of scattered light from SWs existing at a 1DPC–bulk interface by using a modified ATR setup. The high sensitivity of the SW, due to changes in the geometrical parameters of a multilayer, allows us to determine the local (point-by-point) thicknesses of a thin film at the subnanometer scale. With our experimental setup, it is possible to determine the thickness distribution of a thin film along an extended area that is correlated to every pixel of the image associated to each point in the surface of the sample by using an automated post-processing algorithm based on numerical fitting. The use of this technique could be useful for future characterization of SW-based photonic devices on top of 1DPCs.

Funding. Consejo Nacional de Ciencia y Tecnología (250719, 252621).

Acknowledgment. We express our gratitude to M. Christian Albor for the SEM images obtained from our samples.

REFERENCES

1. J. D. Joannopoulos, S. G. Johnson, J. N. Winn, and R. D. Meade, *Photonic Crystals: Molding the Flow of Light*, 2nd ed. (Princeton University, 2008).
2. R. D. Meade, K. D. Brommer, A. M. Rappe, and J. D. Joannopoulos, "Electromagnetic Bloch waves at the surface of a photonic crystal," Phys. Rev. B **44**, 10961 (1991).
3. F. Ramos-Mendieta and P. Halevi, "Electromagnetic surface modes of a dielectric superlattice: the supercell method," J. Opt. Soc. Am. B **14**, 370–381 (1997).
4. J. Homola, "Present and future of surface plasmon resonance biosensors," Anal. Bioanal. Chem. **377**, 528–539 (2003).
5. P. Arora, E. Talker, N. Mazurski, and U. Levy, "Dispersion engineering with plasmonic nano structures for enhanced surface plasmon resonance sensing," Sci. Rep. **8**, 9060 (2018).
6. F. Villa, L. E. Regalado, F. Ramos-Mendieta, J. Gaspar-Armenta, and T. López-Ríos, "Photonic crystal sensor based on surface waves for thin film characterization," Opt. Lett. **27**, 646–648 (2002).
7. V. N. Konopsky and E. V. Alieva, "Photonic crystal surface waves for optical biosensors," Anal. Chem. **79**, 4729–4735 (2007).
8. F. Villa, J. A. Gaspar-Armenta, and F. Ramos-Mendieta, "One-dimensional photonic crystals: equivalent systems to single layers with a classical oscillator like dielectric function," Opt. Commun. **216**, 361–367 (2003).

9. J. A. Gaspar-Armenta and F. Villa, "Band structure properties of one-dimensional photonic crystals under the formalism of equivalent systems," J. Opt. Soc. Am. B **21**, 405–412 (2004).
10. W. M. Robertson, "Experimental measurement of the effect of termination on surface electromagnetic waves in one-dimensional photonic bandgap arrays," J. Lightwave Technol. **17**, 2013–2017 (1999).
11. A. S. Ramírez-Duverger, J. Gaspar-Armenta, and R. García-Llamas, "Experimental determination of a surface wave at the one-dimensional photonic crystal-metal interface," J. Opt. Soc. Am. B **25**, 1016–1024 (2008).
12. M. Shinn and W. M. Robertson, "Surface plasmon-like sensor based on surface electromagnetic waves in a photonic band-gap material," Sens. Actuators B **105**, 360–364 (2005).
13. A. S. Ramirez-Duverger, J. Gaspar-Armenta, and R. García-Llamas, "Surface wave effect on light scattering from one-dimensional photonic crystals," Opt. Commun. **277**, 302–309 (2007).
14. E. Descrovi, F. Giorgis, L. Dominici, and F. Michelotti, "Experimental observation of optical band-gaps for surface electromagnetic waves in a 1D silicon nitride photonic crystal," Opt. Lett. **33**, 243–245 (2008).
15. A. Sinibaldi, N. Danz, E. Descrovi, P. Munzert, U. Schulz, F. Sonntagd, L. Dominicia, and F. Michelotti, "Direct comparison of the performance of Bloch surface wave and surface plasmon polariton sensors," Sens. Actuators B **174**, 292–298 (2012).
16. D. A. Shilkin, E. V. Lyubin, I. V. Soboleva, and A. A. Fedyanin, "Photonic force microscopy of surface electromagnetic waves in a one-dimensional photonic crystal," Proc. SPIE **9548**, 954810 (2015).
17. E. Descrovi, D. Morrone, A. Angelini, F. Frascella, S. Ricciardi, P. Rivolo, N. De Leo, L. Boarino, P. Munzert, F. Michelotti, and F. Giorgis, "Fluorescence imaging assisted by surface modes on dielectric multilayers," Eur. Phys. J. D **68**, 53 (2014).
18. H. Morgan and D. M. Taylor, "Surface plasmon resonance microscopy: reconstructing a three-dimensional image," Appl. Phys. Lett. **64**, 1330 (1994).
19. C. E. García-Ortíz, R. Cortes, R. Orejel, R. Hernández-Aranda, I. Martínez-López, F. Aguilar, and V. Coello, "3D thickness map reconstruction of dielectric thin films using scattering of surface plasmon polaritons," Opt. Lett. **43**, 691–694 (2018).
20. A. Drezet, A. Hohenau, D. Koller, A. Stepanov, H. Ditlbacher, B. Steinberger, F. R. Aussenegg, A. Leitner, and J. R. Krenn, "Leakage radiation microscopy of surface plasmon polaritons," Mater. Sci. Eng. B **149**, 220–229 (2008).
21. R. Dubey, E. Barakat, M. Häyrinen, M. Roussey, S. K. Honkanen, M. Kuittinen, and H. P. Herzig, "Experimental investigation of the propagation properties of Bloch surface waves on dielectric multilayer platform," J. Eur. Opt. Soc. **13**, 5 (2017).

158.97.112.15 {ts '2019-09-05 14:08:51'}